# Programmable Matrix-Array Thermoelectric System With Tri-State Energy Conversion

Ning Wang, *Senior Member, IEEE*,
Hong-Tao Huang, Lei Zhang, Shu-Xi Xu, Yuan Liu, Hong-Zhi Jia, and Guan-Xue Wang

***Abstract*—This article presents a matrix-arranged thermoelectric programmable control system. The system flexibly reconfigures the functions of each thermoelectric module in the matrix, overcoming the limitations of unidirectional energy flow and fixed functionality in traditional thermoelectric systems. By constructing a three-state (cooling/heating/energy harvesting) reconfigurable topology, distributed cooperative control of temperature management and energy recovery in nonuniform thermal fields is realized. A dynamic temperature management strategy based on the fuzzy-PID algorithm is adopted, allowing the region's temperature to converge rapidly. Experimental results indicate that, compared to conventional methods, the proposed system achieves a temperature error of only 1.72 °C, reduces convergence time by 50.88%, and improves temperature conversion efficiency by up to 92.57%. In energy harvesting mode, the system achieves a maximum captured voltage of 320 mV, with a ripple rate below 1.6% after boosting to 5 V, and a peak power density of $7.24 \times 10^{-5}$ W/cm$^2$K. This work provides an efficient and energy-consistent integrated solution for semiconductor cooling, industrial thermal management, and other applications.**

***Index Terms*—Dynamic temperature management, energy capture, fuzzy-PID, programmable thermal control.**

## I. Introduction

GLOBAL energy consumption primarily relies on nonrenewable fossil fuels [1], [2], whose carbon emissions not only cause severe pollution but also contribute to global warming [3], [4]. At present, key energy-consuming sectors, including industrial equipment, building environments, and transportation [5], [6], [7], [8], are driving a low-carbon transition by utilizing green energy sources such as solar and geothermal energy. However, the ongoing heat losses in this process intensify energy waste, causing local thermal imbalance and system performance degradation, which creates a vicious cycle of energy consumption and system decay [9], [10], [11]. Therefore, the development of new mechanisms that integrate both thermal management and energy conversion has become imperative.

Thermoelectric technology, as a pollution-free, noiseless, and easy-to-control solid-state energy conversion technology, takes advantage of its bidirectional "heat-to-electricity" conversion to efficiently recover low-grade thermal energy, such as industrial waste heat and building heat waste [12], [13], and to utilize thermoelectric reversibility to meet the temperature control needs of electric vehicle batteries, large solar panels (PV) [14], [15], etc., by combining Thermoelectric cooler-Thermoelectric generator (TEC-TEG), achieving on-demand thermal control and waste heat recovery. In contrast to traditional passive thermal management methods, this technology mitigates the risk of thermal runaway while converting waste heat into a crucial energy source that drives the system's self-sustaining operation.

TEC employs the Peltier effect, controlling the current direction to efficiently manage localized heat sources [16], [17]. For instance, Zhang et al. [18] applied partial TEC precooling technology and developed a 4.5-kV power electronic switch module prototype with an integrated precooling device, resulting in a 15 °C temperature reduction for internal components and about a 10% enhancement in current performance. Compared to single-stage TEC, multistage TEC achieves higher cooling efficiency and lower temperature by optimizing module size and current control: Buchalik et al. [17] achieved temperature reduction and maximized subcooling with a two-stage thermoelectric module (TEM), while Zhang et al. [19] achieved a minimum temperature of −82.15 °C and a cooling power density of up to 4 kW/m$^2$ through precise control of the optimal operating current for each stage. Nevertheless, while meeting high-power temperature control demands, multistage TEC tends to produce excess waste heat. Leveraging the Seebeck effect, TEM can convert this excess heat into electrical energy, and the reconfigurable design of multistage thermoelectric arrays (Thermoelectric Array, TEA) [20], [21] enhances overall energy efficiency. For example, Yousri et al. [22] utilized the Rime

Received 18 January 2025; revised 28 March 2025; accepted 25 April 2025. Date of publication 30 April 2025; date of current version 30 June 2025. The work of Ning Wang, Hong-Tao Huang, Lei Zhang, Shu-Xi Xu, Yuan Liu, and Hong-Zhi Jia was supported in part by the National Natural Science Foundation of China under Grant 62474112, in part by Shanghai Pujiang Programme under Grant 23PJD066, and in part by the National Science and Technology Major Project from Minister of Science and Technology, China, under Grant 2018AAA0103100. This work was supported by the Engineering Research Center of Optical Instrument and System, Ministry of Education, Shanghai Key Laboratory of Modern Optical System, University of Shanghai for Science and Technology, Shanghai, China. Recommended for publication by Associate Editor S. Jeong. *(Corresponding author: Guan-Xue Wang.)*

Ning Wang, Hong-Tao Huang, and Hong-Zhi Jia are with the Engineering Research Center of Optical Instrument and System Ministry of Education, Shanghai Key Laboratory of Modern Optical System, University of Shanghai for Science and Technology, Shanghai 200093, China (e-mail: nwang@usst.edu.cn).

Lei Zhang, Shu-Xi Xu, and Yuan Liu are with the 214 Institute of China North Industries, Suzhou 215163, China (e-mail: 223330853@st.usst.edu.cn; 223330720@st.usst.edu.cn; yuan.liu@smail.nju.edu).

Guan-Xue Wang is with the School of Energy and Power Engineering, University of Shanghai for Science and Technology, Shanghai 200093, China (e-mail: wangguanxue@usst.edu.cn).

This article has supplementary material provided by the authors and color versions of one or more figures available at https://doi.org/10.1109/TPEL.2025.3565763.

Digital Object Identifier 10.1109/TPEL.2025.3565763

Optimization Algorithm (RIME) to dynamically reconfigure the TEG array (including series-parallel, fully crosslinked, bridge-linked, honeycomb, and other configurations), improving output power and efficiency in nonuniform thermal fields, with the bridge-linked design even enhancing output power by up to 5%.

Existing systems are mostly based on single-function TEM designs, failing to integrate TEG and TEC to achieve on-demand temperature control, and struggle to meet large-area temperature control demands [23], [24], [25]. To this end, in our earlier research, our team developed a rapid temperature control system for automotive batteries using an optimized Fuzzy-PID algorithm [23]. The system employs switchable TEM and liquid cooling assistance, reducing the temperature control time by about 76% compared to multichannel liquid cooling. The thermal runaway group can reduce the temperature from 63.5 to 25 °C in 280 s, while the freezing group can increase the temperature from −10 to 25 °C in 185 s. Meanwhile, our proposed intelligent thermal management PV-TEH system [24] achieves precise control of photovoltaic panel temperature by unifying TEM and PWM cooling adjustment. It not only improves the conversion efficiency to 27.8%, reducing the temperature of the photovoltaic panel by 6 °C, but also extends the pure power supply time window in PV-TEG mode and increases the effective output power from 6 to 8.1 W in PV-TEC mode. In addition, the Kim et al. [15] constructed an array using 12 TEMs to develop an integrated automotive energy recovery system. The system generates electricity from exhaust heat via TEG and drives the TEC to reduce the interior temperature of the car from 45 to 26 °C in 3 min.

However, existing combined thermoelectric systems still have significant shortcomings: mode switching relies on global control, unable to dynamically adjust the state of individual modules based on local temperatures, resulting in energy loss in nontarget areas; the fixed layout of TEC and TEG is difficult to adapt to the spatial distribution of nonuniform heat fields; and there is a lack of real-time programming capability for TEM operating states, making it difficult to achieve coordinated balance between temperature control and energy recovery.

To solve the above-mentioned issues, this article designs a matrix-based thermoelectric multiplexing programmable control system to achieve efficient temperature management and energy collection. The system dynamically switches the TEM working modes based on the temperature of each hotspot region and reconstructs local heat flow paths in real-time to adapt to the spatial distribution of nonuniform heat fields. By autonomous decision-making, each region reaches its optimal working state, effectively eliminating energy dissipation in nontarget areas as seen in traditional schemes while simultaneously performing hotspot cooling and waste heat capture. The integrated energy recovery technology successfully captures and converts micro-temperature difference waste heat into usable power, establishing a cooperative channel for temperature gradient suppression and energy feedback, thereby realizing closed-loop control of heat field homogenization and energy regeneration. Section II introduces TEM, Fuzzy-PID control, and red-black tree data structures. Section III details the polymorphic multiplexing design of the TEA. Section IV assesses system performance through experimental results, while Section V concludes this article.

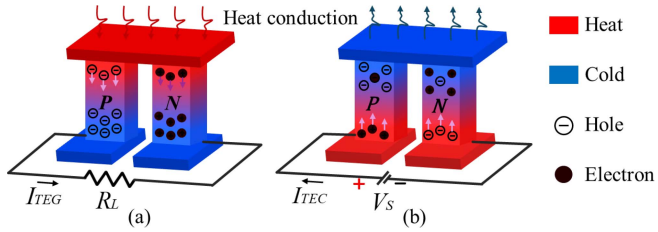


Fig. 1. (a) TEG model. (b) TEC model.

## II. Principles and Theory

### A. Thermoelectric Effect

The thermoelectric effect describes the phenomenon of energy conversion between temperature gradient and electrical potential difference through specific materials, where the essence lies in the diffusion and migration of charge carriers under a temperature gradient [26], [27]. As illustrated in Fig. 1, the TEM is composed of a bridge-coupled unit formed by P-type and N-type semiconductor arms, arranged in thermal parallel and electrical series connections. When a temperature difference is applied across the two sides, the charge carriers (electrons and holes) at the hot end are thermally excited, creating a concentration gradient. This drives the directional migration of charges to balance the chemical potential, ultimately generating an internal built-in electric potential field within the material.

As shown in Fig. 1(a), in power generation mode, the temperature difference $\Delta T$ drives P-type and N-type charge carriers to diffuse towards the cold end, producing a thermoelectric generation current $I_{\mathrm{TEG}}$ that drives the load resistance $R_L$ to supply electrical power. This process is based on the Seebeck effect, and its open-circuit voltage $V_{\mathrm{oc}}$ satisfies

$$V_{\mathrm{oc}} = S\Delta T \tag{1}$$

where $S$ is the Seebeck coefficient between the materials, which is a critical parameter for evaluating the thermoelectric conversion capability.

In Fig. 1(b), in the cooling mode, the applied voltage $V_S$ forces the current $I_{\mathrm{TEC}}$ to drive charge carriers to migrate in reverse, causing heat absorption at the cold end and heat release at the hot end, thereby achieving active cooling. This process depends on the Peltier effect [28], and the heat flow rate per unit time is proportional to $I_{\mathrm{TEC}}$. The cooling performance is determined by the heat absorbed at the cold end $Q_c$, the equivalent thermal conductivity $K$, and the temperature difference $\Delta T = T_h$ - $T_c$, with its coefficient of performance COP defined as

$$\mathrm{COP} = \frac{Q_c}{P_{\mathrm{TEC}}} = \frac{\mathrm{SI}_{\mathrm{TEC}} T_C - \frac{1}{2} I_{\mathrm{TEC}}^2 R_{\mathrm{TEC}} - K\Delta T}{P_{\mathrm{TEC}}} \tag{2}$$

where $T_h$ and $T_c$ represent the temperatures of the hot and cold ends, respectively. The Peltier effect forms the physical basis of solid-state cooling technology.

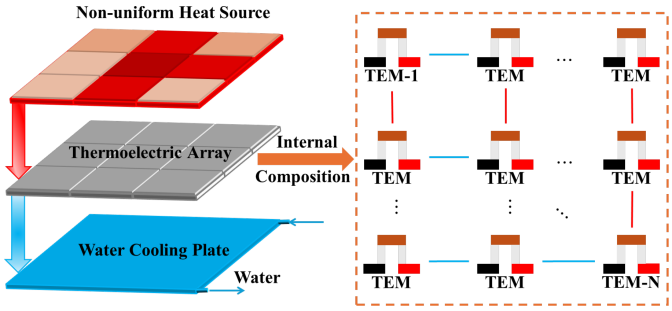


Fig. 2. Thermoelectric-liquid cooling hybrid cooling system for nonuniform thermal field regulation.

### B. Power Calculation of TEA System

As shown in Fig. 2, in response to nonuniform thermal fields, the TEA system is composed of $N$ TEMs, working in conjunction with liquid cooling technology to enhance the TEC temperature control efficiency and the temperature difference of the TEG. The total number of TEMs, $N$, is made up of the controllable numbers of TEGs, $N_{\mathrm{TEG}}$, and TECs, $N_{\mathrm{TEC}}$

$$N = N_{\mathrm{TEG}} + N_{\mathrm{TEC}}. \tag{3}$$

In the power generation mode, the $N_{\mathrm{TEG}}$ TEGs in the TEA are connected in series. According to (1), the captured voltage $V_{\mathrm{TEG}}$ and $I_{\mathrm{TEG}}$ are as

$$V_{\mathrm{TEG}} = \sum_{n=1}^{N_{\mathrm{TEG}}} V_{\mathrm{TEG}}(n) = S(n) \sum_{n=1}^{N_{\mathrm{TEG}}} \Delta T_{\mathrm{TEG}}(n) \tag{4}$$

$$I_{\mathrm{TEG}} = \frac{V_{\mathrm{TEG}}}{R_{\mathrm{TEG}} + R_L} = \frac{S(n)\sum_{n=1}^{N_{\mathrm{TEG}}} \Delta T_{\mathrm{TEG}}(n)}{\sum_{n=1}^{N_{\mathrm{TEG}}} R_{\mathrm{TEG}}(n) + R_L} \tag{5}$$

where $V_{\mathrm{TEG}}(n)$ and $R_{\mathrm{TEG}}(n)$ represent the open-circuit voltage and internal resistance of the $n$th TEG, respectively; $S(n)$ and $\Delta T_{\mathrm{TEG}}(n)$ are the total $S$ and the temperature difference across the terminals of the $n$th TEG, respectively; $R_L$ denotes the load resistance.

The output power of the energy harvesting module TEG can be calculated using the following equation:

$$P_{\mathrm{TEG}} = I_{\mathrm{TEG}}^2 R_L = S(n) \sum_{n=1}^{N_{\mathrm{TEG}}} \left( \frac{\Delta T_{\mathrm{TEG}}(n)}{R_{\mathrm{TEG}}(n) + R_L} \right)^2 R_L. \tag{6}$$

In the cooling mode, the current control of the TEC usually works in conjunction with the H-bridge circuit. After applying the PWM wave with a duty cycle of $D(k)$ to the H-bridge, the total voltage experienced by the TEC is the sum of the system supply voltage $V_s$ and the reverse voltage $V_{\mathrm{TM}}(k)$ generated by the TEG. The current $I_{\mathrm{TEC}}(k)$ of the TEC unit is

$$\begin{aligned} I_{\mathrm{TEC}}(k) &= \frac{V_S D(k) - V_{\mathrm{TM}}(k)}{R_{\mathrm{TEC}}(k) + R_{\mathrm{IN}}} \\ &= \frac{V_S D(k) - S(k)\Delta T_{\mathrm{TEC}}(k)}{R_{\mathrm{TEC}} = \sum_{k=1}^{N_{\mathrm{TEC}}} R_{\mathrm{TEC}}(k) + R_{\mathrm{IN}}} \end{aligned} \tag{7}$$

where $R_{\mathrm{TEC}}$ represents the total internal resistance of the system's TEC at the given moment; $R_{\mathrm{TEC}}(k)$, $S(k)$, and $\Delta T_{\mathrm{TEC}}(k)$ refer to the internal resistance, total $S$, and the temperature difference across the terminals of the $k_{\mathrm{th}}$ TEC, respectively; $R_{\mathrm{IN}}$ is the internal resistance of the system power supply.

Consequently, the total power consumed by all TEC units at a specific moment can be calculated as

$$\begin{aligned} P_{\mathrm{TEC}} &= I_{\mathrm{TEC}}^2 R_{\mathrm{TEC}} \\ &= \sum_{k=1}^{N_{\mathrm{TEC}}} \left( \frac{V_S D(k) - S\Delta T_{\mathrm{TEC}}(k)}{R_{\mathrm{TEC}}(k) + R_{\mathrm{IN}}} \right)^2 R_{\mathrm{TEC}}(k). \end{aligned} \tag{8}$$

The conversion efficiency of the entire system reflects its ability to convert absorbed energy into other forms of energy. By the collaborative operation of the TEG/TEC heterogeneous array, the system creates a bidirectional energy conversion network: the TEG module generates Seebeck voltage using the temperature difference, while the TEC module achieves local cooling through the Peltier effect. The effective energy factor $\xi$ is defined as $\xi = P_{\mathrm{TEC}\text{-}P}/P_{\mathrm{TEC}\text{-}N}$, which represents the effective cooling power corresponding to unit irreversible energy consumption. In the nonequilibrium state, the temperature conversion efficiency $\eta$ is given by

$$\begin{aligned} \eta &= \frac{P_{\mathrm{TEC}-P} - P_{\mathrm{TEG}}}{P_{\mathrm{TEC}-N} + P_{\mathrm{TEC}-P} - P_{\mathrm{TEG}}} \\ &= \frac{1}{1 + (\xi + P_{\mathrm{TEG}}/P_{\mathrm{TEC}-P})^{-1}} \end{aligned} \tag{9}$$

where $P_{\mathrm{TEC}\text{-}N}$ is associated with losses from thermal management delay, control overshoot, and parasitic heat conduction, while $P_{\mathrm{TEC}\text{-}P}$ represents the effective heat transport power in the target temperature zone.

### C. Fuzzy-PID Algorithm

PID control achieves dynamic adjustment based on proportional, integral, and derivative actions and is widely used in continuous control systems [29]. However, in systems with large delays, strong nonlinearity, and frequent disturbances, such as temperature management, an incremental PID algorithm with antisaturation and antidisturbance properties is required

$$\Delta u_k = K_p(e_k - e_{k-1}) + K_i e_k + K_d(e_k - 2e_{k-1} + e_{k-2}) \tag{10}$$

where $K_p$, $K_i$, and $K_d$ represent the proportional, integral, and derivative coefficients, respectively; $e_k$, $e_{k\text{-}1}$, and $e_{k\text{-}2}$ represent the errors at the $k_{\mathrm{th}}$, $k$-$1_{\mathrm{th}}$, and $k$-$2_{\mathrm{th}}$ instances.

To address the issue of linear PID failure caused by the time-varying characteristics of temperature systems, the fuzzy-PID algorithm adaptively adjusts the PID parameters through fuzzy reasoning, effectively overcoming system nonlinearity and uncertainty [23]. As shown in Fig. 3, its core process includes three stages: fuzzification, rule inference, and defuzzification. First, the temperature error and its rate of change are fuzzified into linguistic variables, and the corresponding control strategy is activated based on the constructed rule base. Then, defuzzification methods, such as the centroid method, are used to output

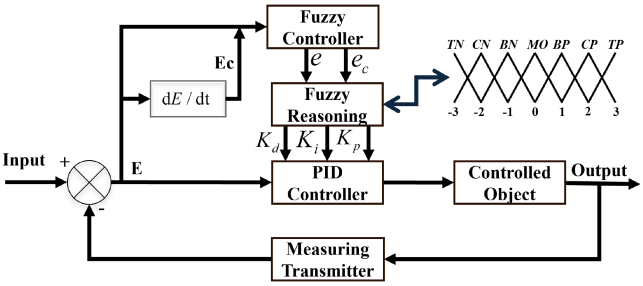


Fig. 3. Control principle of the fuzzy-PID algorithm.

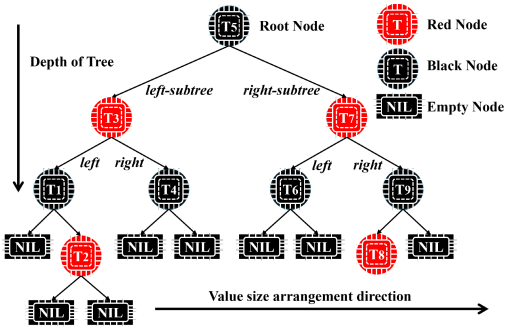


Fig. 4. Structure of the red-black tree.

the correction amounts for $\Delta K_p$, $\Delta K_i$, and $\Delta K_d$ parameters, and the PID gains are updated in real-time based on the membership function parameters and fuzzy-PID boundary constraints. The numbers –3 to 3 map normalized errors (0 = neutral; ±3 = large deviations). Labels such as TN, CN, BN are linguistic variables that drive the fuzzy adjustment of PID parameters.

### D. Red-Black Tree Data Structure

In thermoelectric systems, the red-black tree, due to its self-balancing and efficient retrieval properties, is an ideal choice for managing temperature gradient data. As shown in Fig. 4, this data structure employs red-black coloring (with the root and leaves black, and red nodes noncontiguous) and dynamic rotations, keeping the tree height stable within the range of $2\log(n+1)$ [30]. All temperature nodes are arranged according to the in-order traversal rule, meaning they are sorted in ascending order and are embedded with TEM data, allowing for logarithmic-level complexity in insertion, sorting, and querying.

According to (11), real-time temperature data is collected by starting at the root node, and the insertion position is determined via binary comparisons across layers. This method reduces the traditional traversal time from $O(n)$ to $O(\log n)$, achieving a microsecond-level response. The efficiency is attributed to the strict balance maintained by the number of black nodes along the path in the red-black tree. Imbalances are automatically corrected through color flipping and subtree rotation, ensuring that TEA temperature data is stored in a real-time and orderly manner

$$T_{\text{insert}} \in \begin{cases} \text{left} - \text{subtree}, \text{T}_{\text{insert}} < \text{node.key} \\ \text{right} - \text{subtree}, \text{T}_{\text{insert}} > \text{node.key} \end{cases}. \tag{11}$$

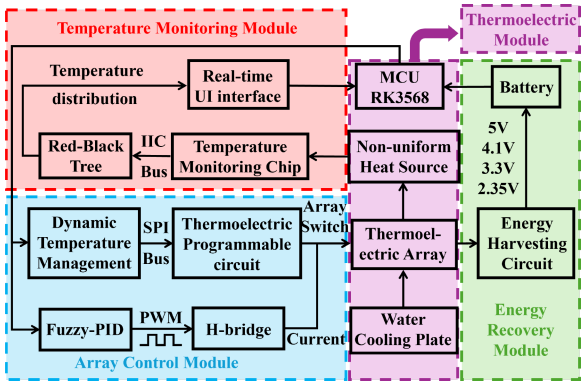


Fig. 5. Framework of the TEA three-state programmable reuse system.

## III. Tri-State Programmable Multiplexing System of TEA

To solve the issue of traditional fixed TEC/TEG layouts failing to cope with uneven temperature field distributions and energy loss in nontarget areas, this study presents a dynamic programmable TEA three-state reusable system (see Fig. 5). The system reconfigures the operating mode of TEMs dynamically, dividing the array into TEC and TEG functional zones: the TEC zone implements precise temperature control to suppress local heat buildup, while the TEG zone recovers waste heat for power generation, minimizing parasitic losses.

### A. Intelligent Mode Switching of TEM

To achieve programmable dynamic reconfiguration of the array, this article proposes an intelligent switching technology for the three states (cooling/heating/energy recovery) of thermoelectric reuse. Single-stage TEM mode switching relies on the collaborative control of relays and H-bridge: the $\text{SIG}_{\text{OH}}$ signal controls each column of TEMs to switch to TEC mode, while the $\text{SIG}_{\text{OL}}$ signal controls each row of TEMs. Both signals together determine the relay state, thereby deciding whether the TEM switches to TEC mode. Simultaneously, the DIR signal indicates the current direction of TEMs and controls the H-bridge's ON/OFF state. Finally, the three-state control signal $Z$ is generated by two XOR gates and an AND gate combining $\text{SIG}_{\text{OH}}$, $\text{SIG}_{\text{OL}}$, and DIR, i.e., $Z = (\text{SIG}_{\text{OH}} \oplus \text{SIG}_{\text{OL}}) \bullet (\text{SIG}_{\text{OL}} \oplus \text{DIR})$. The mode switching logic is shown in Table I. Initially, $Z = 0$, the relay is open, and the TEM operates in TEG mode. When the row and column signals are in opposite phases ($\text{SIG}_{\text{OH}} \oplus \text{SIG}_{\text{OL}} = 1$) and consistent with DIR(DIR = 1 directs current from $\text{SIG}_{\text{OH}}$ to $\text{SIG}_{\text{OL}}$, while DIR = 0 reverses it), the H-bridge drives the TEM into TEC mode, with the cooling or heating direction determined by DIR.

As shown in Fig. 6, the control process of a single-stage TEM in three states is as follows: when the input serial data is 101 (DIR = 1) [see Fig. 6(a)], the H-bridge outputs forward current to make the TEC enter the cooling mode. At this point, the cold end of the TEC contacts the temperature field to lower the temperature, while the hot end expels heat via the water-cooling plate. When the input data is 010 (DIR = 0) [see Fig. 6(b)], the

TABLE I
CONTROL LOGIC TABLE FOR SINGLE-STAGE TEM

| Serial Data | $SIG_{OH}$ | $SIG_{OL}$ | DIR | H-Bridge | Relay | Function |
|---|---|---|---|---|---|---|
| 000 | 0 | 0 | 0 | High-resistivity | Turn-OFF | TEG |
| 010 | 0 | 1 | 0 | Reverse Current | Turn-ON | TEC Heating |
| 011 | 0 | 1 | 1 | Reverse Current | Turn-OFF | TEG |
| 100 | 1 | 0 | 0 | Forward Current | Turn-OFF | TEG |
| 101 | 1 | 0 | 1 | Forward Current | Turn-ON | TEC Cooling |
| 110 | 1 | 1 | 0 | High-resistivity | Turn-OFF | TEG |
| 111 | 1 | 1 | 1 | High-resistivity | Turn-OFF | TEG |

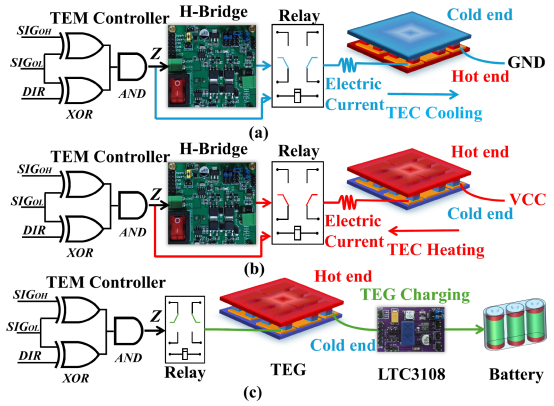


Fig. 6. Tri-state control of single-stage TEM. (a) TEC cooling mode. (b) TEC heating mode. (c) TEG energy harvesting mode.

H-bridge outputs reverse current, switching the TEC into heating mode. The hot end of the TEC heats the temperature field, while the cold end prevents condensation using the water-cooling plate. In both modes, the signal $Z$ is positive, which allows the relay to close, and the system enters the active temperature control state, with the H-bridge providing voltage to drive the TEC. Other data combinations produce a negative signal $Z$, as shown in Fig. 6(b), causing the relay to open, and the system automatically switches to TEG mode. The temperature difference is utilized by the LTC3108 circuit to supply power to low-power devices and batteries, enabling bidirectional recycling of thermal and electrical energy.

### B. TEA Integrated Control System

In the single-stage TEM control method described above, using the array connection shown in Fig. 7(a), only X+Y control signals are required to program and control X•Y TEAs. As illustrated in Fig. 7(b), when $SIG_{OH}$-1 to $SIG_{OH}$-X are set to "10…0", $SIG_{OL}$-1 to $SIG_{OL}$-Y are set to "00…0", and DIR = 1, all TEMs in the $SIG_{OH}$-1 column switch to TEC mode, while the remaining TEMs remain in TEG mode, thus enabling the parallel operation of TEC and TEG.

Based on the intelligent reuse of TEM, Fig. 8 presents the TEA integrated control system, which is composed of three main units: central computation, temperature management, and energy collection. The microcontroller unit (MCU) retrieves temperature information from the TEA temperature distribution data stored in the red-black tree and uses the fuzzy-PID algorithm to dynamically control the temperature of the target surface, identifying critical regions requiring precise management. The MCU then generates analytical data and transmits parallel control instructions to the temperature management unit via SPI. After parsing the instructions, the unit produces control signals through logical operations and sends them to the H-bridge circuit and array control board, precisely regulating the working state of each TEM to achieve accurate temperature regulation in the specified area. Simultaneously, waste heat not managed by the temperature control system is converted into electrical energy by the energy collection module and stored in the battery, ensuring effective energy recovery and reuse.

### C. Dynamic Temperature Management

In the presence of nonuniform heat sources, TEC thermal management faces the issue of temperature diffusion. A weighted method can be employed to identify key regions for temperature management, as illustrated in Fig. 9. This method begins by analyzing the overall temperature error gradient and calculating the temperature distribution ratio $K_i$ for each region to assess the intensity of its thermal control requirements. By multiplying the error $E_i$ of each region with its corresponding distribution ratio $Ki$, the priority $M_i$ of potential hotspot regions is determined, allowing precise identification of areas requiring urgent temperature regulation. This approach not only effectively addresses complex temperature distributions and achieves optimal control performance but also leverages natural temperature diffusion to minimize system energy consumption.

The critical temperature control point $M_m$, identified using this method, is managed automatically via the dynamic temperature management algorithm illustrated in Fig. 10. The system first determines whether the temperature error $Em$ at the point meets or exceeds the threshold $E_{\min}$. If $E_m < E_{\min}$, a specific configuration signal is transmitted to adjust TEA. Next, $Em$ and its rate of change $\Delta E_m$ are fed into the fuzzy-PID controller to update the PID parameters (as detailed in Algorithm 1). A PWM signal is then configured to control the H-bridge output current to the TEC, effectively managing nonuniform temperature regions. If $E_m > E_{\min}$, the system ceases temperature management.

## IV. RESULTS AND DISCUSSION

### A. System Environment Setup

To verify the effectiveness of the proposed system, an experimental platform was constructed, as shown in Fig. 11. It mainly

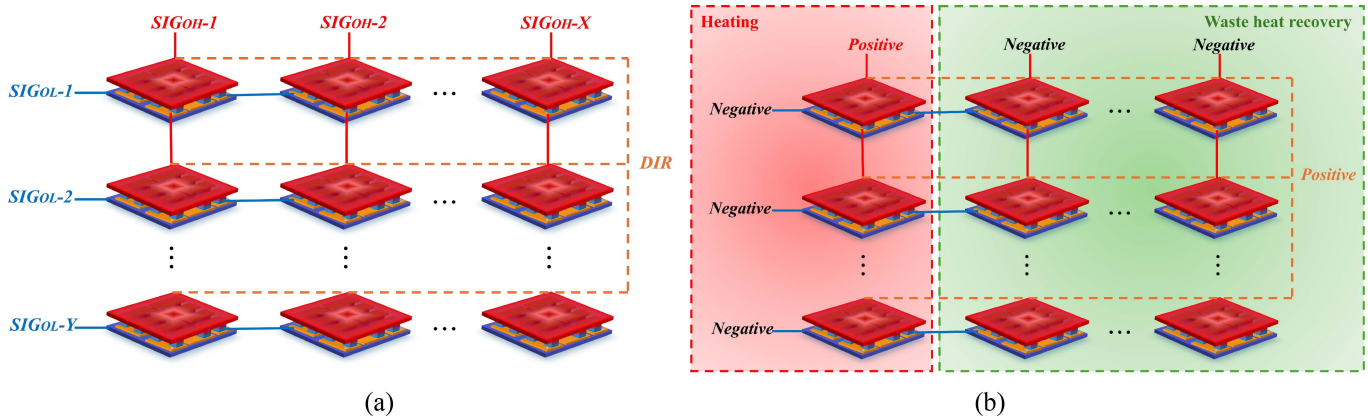


Fig. 7. (a) Array connection method. (b) Operating modes of each TEM in the TEA when the control signals $SIG_{OH}$-1 to $SIG_{OH}$-X are 10…0, $SIG_{OL}$-1 to $SIG_{OL}$-Y are 00…0, and DIR = 1.

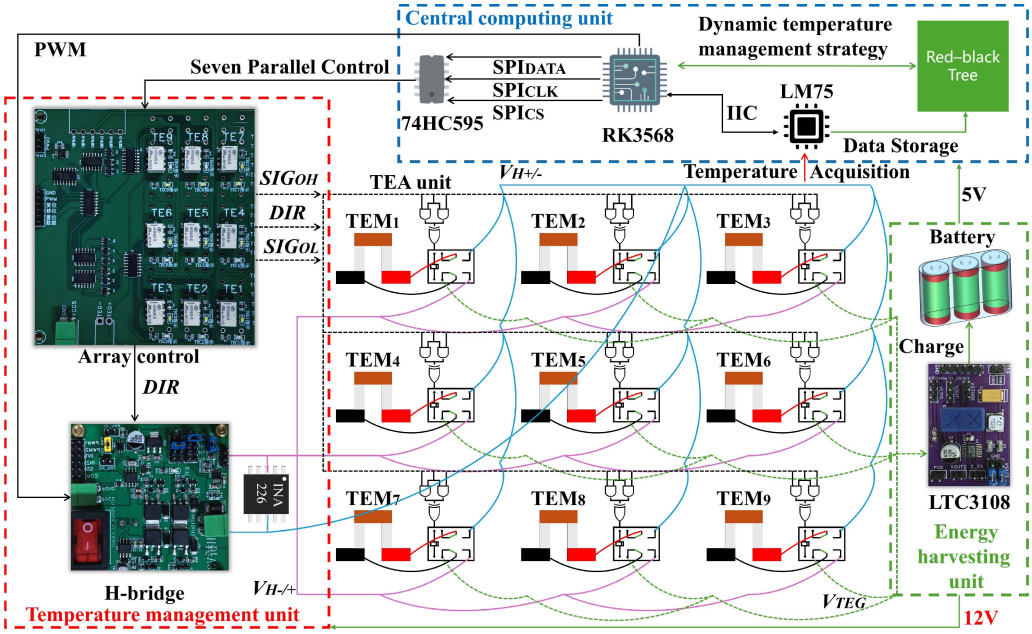


Fig. 8. TEA integrated control.

comprises a TEA module, a display device, a thermoelectric control module, and peripheral devices for energy harvesting and storage. The TEA module consists of nine TEM and an associated water-cooled heat dissipation system. The devices are coupled together with thermal grease to form a square array. The system also includes a display device that visually presents key experimental parameters, such as temperature, power, and the operating status of each TEM in the array. As the core of the system, the thermoelectric control module enables programmable control of the TEA, managing both temperature regulation and energy harvesting. This module is primarily composed of an MCU, an H-bridge circuit, an energy harvesting circuit, and a TEM programmable circuit. The parameters of these experimental devices are detailed in Table II.

### B. Temperature Management

Based on the system hardware test platform, we conducted a comparative experiment between the array control mode and the traditional control mode. The experimental area was divided into nine adjacent temperature regions (Section 1–9), each corresponding to different temperature distributions ($T_1$–$T_9$). In the traditional mode, the thermoelectric system consists of three TECs connected in series to form a unit, and three such units are connected in parallel, with a relatively fixed functionality and connection method as shown in Fig. 12. In the array mode, nine programmable TEMs can be independently controlled, providing adaptive control capabilities. The main differences between the two modes are shown in Table III.

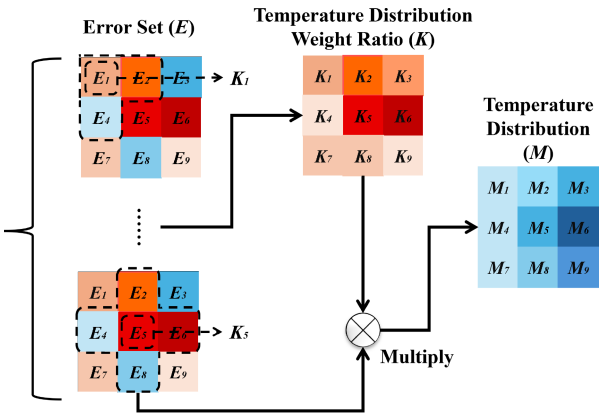


Fig. 9. Tracking of temperature-sensitive points.

**Algorithm 1:** Fuzzy Control Logic.

**Output:** Adjusted PID parameters $\Delta K_p$, $\Delta K_i$, $\Delta K_d$;

**Input:**

- Error $(e)\in[-E_{\max}, E_{\max}]$;
- Error change $(\dot{e})\in[-\Delta E_{\max}, \Delta E_{\max}]$;
- Fuzzy structure (fuzzy_struct);

**Initialize**:

- Membership arrays $\mu_e[\cdot]$, $\mu_{\dot{e}}[\cdot]$;
- Active rule indices $idx_e[\cdot]$, $idx_{\dot{e}}[\cdot]$;
- Joint membership matrix $\mu_{\text{joint}}[\cdot]$;

**Steps:**

1. **Normalization:**
Map inputs to normalized domain $[-11]$:
$$e_{\text{norm}} = \frac{e}{E_{\max}}$$
$$\dot{e}_{\text{norm}} = \frac{\dot{e}}{\Delta E_{\max}}$$
2. **Fuzzification:**
Compute membership degrees for $e_{\text{norm}}$ and $\dot{e}_{\text{norm}}$:
$$\mu_e[i] = \text{trim}f(e_{\text{norm}}, a_i, b_i, c_i)$$
$$\mu_{\dot{e}}[i] = \text{trim}f(\dot{e}_{\text{norm}}, a'_i, b'_i, c'_i)$$
Prune $\mu_e$, $\mu_{\dot{e}}$ with $\mu < 0.0001$.
Store valid memberships and indices:
$idx_e[\cdot]\leftarrow\{i|\mu_e[i] \geq 0.0001\}$, $idx_{\dot{e}}[\cdot]\leftarrow\{j|\mu_{\dot{e}}[j] \geq 0.0001\}$.
3. **Rule Activation:**
For each pair $(i, j) \in idx_e \times idx_{\dot{e}}$:
Retrieve consequent fuzzy set $C^k{}_{i,j}$ from partitioned rule base $R_p$, $R_i$, $R_d$ ($\Delta K_p$, $\Delta K_i$, $\Delta K_d$ blocks).
Compute activation strength $\mu_{\text{joint}}$:
$\mu_{\text{joint}}[i, j] = \min(\mu_e[i], \mu_{\dot{e}}[j])$.
4. **Defuzzification:**
For each PID parameter $\Delta K_*$:
$$\Delta K_* = \frac{\sum(\mu_{\text{joint}}[k]\cdot C_k)}{\sum \mu_{\text{joint}}[k]}$$
$C_k$: Centroid value of output fuzzy set
(e.g., $C_{\text{NB}} = -1.0$, $C_{\text{PB}} = 1.0$).
5. **Parameter Clipping:**
$$\Delta K_* = \text{clip}(\Delta K_*, \Delta K_*^{\min}, \Delta K_*^{\max})$$
Limits defined by the max and min of each PID parameter.

TABLE II
RELEVANT PARAMETERS OF THE EXPERIMENTAL SETUP

| Device | Parameter | Value |
|---|---|---|
| TEM | Type | TEC1-12704 |
| | Size | 40 × 40 × 4.0 mm |
| | Rated voltage | 12 V |
| | Cooling power | 35 W |
| 74HC595D | Size | 10.3 mm × 7.5 mm × 1.27 mm |
| | Bit width | 8 Bit |
| | Maximum operating frequency | 25 MHz |
| INA226 | Size | 3 mm × 4.9 mm × 1.0 mm |
| | ADC native resolution | 16 Bit |
| | Fastest conversion time | 140 µs |
| | Power measurement accuracy | 0.2 % |
| LM75A | Size | 2 mm × 2.3 mm × 1 mm |
| | ADC native resolution | 11 Bit |
| | Temperature resolution | 0.125 °C |
| LTC3108 | Size | 7.8 mm × 6.1 mm × 2 mm |
| | Minimum input voltage | 20 mV |

TABLE III
COMPARISON OF MODE DIFFERENCES

| Mode | TEM connection mode | Number of units | Control flexibility |
|---|---|---|---|
| Tradition | Series-parallel | Three parallel units (Three TECs in series per unit) | Fixed control policy |
| Array | Programmable | Nine independent TEMs | Highly programmable and adaptive control |

As depicted in Fig. 13(a), the initial temperature field follows a radial distribution (28–51 °C), with the central region $T_{T\text{-}3}$ exhibiting the highest temperature. The initial total error is $E_{\text{total}} = 83.31$ °C. Using $T_{T\text{-}3}$ as a reference, the target temperature is set to $T_{\text{target}} = 25$ °C (optimal operating temperature), and a fuzzy-PID control strategy is implemented for thermal regulation. The experimental results under different control modes, shown in Fig. 13(d) and (e), reveal that in the red-marked regions, all TECs effectively transport heat toward $T_{\text{target}}$, achieving a stable 25 °C without overshoot. Moreover, $P_{\text{TEC-}P} > P_{\text{TEC-}N}$ and $\xi$ shows a notable increase, indicating that the array efficiently tracks hotspots and enables precise thermal control, reducing overshoot, shortening regulation time, and minimizing energy consumption. In contrast, the blue-marked regions exhibit ineffective heat transfer due to excessive TEC cooling ($P_{\text{TEC-}P}<P_{\text{TEC-}N}$, leading to a decrease in $\xi$), causing delayed temperature regulation and increased power consumption.

The fundamental drawback of the conventional control mode arises from the rigid operational characteristics of TEM units. As depicted in Fig. 13(d), forcibly cooling $T_{\text{T-3}}$ to $T_{\text{target}}$ induces a reverse thermal gradient due to continuous cooling in surrounding regions, resulting in localized ineffective heat transfer. This

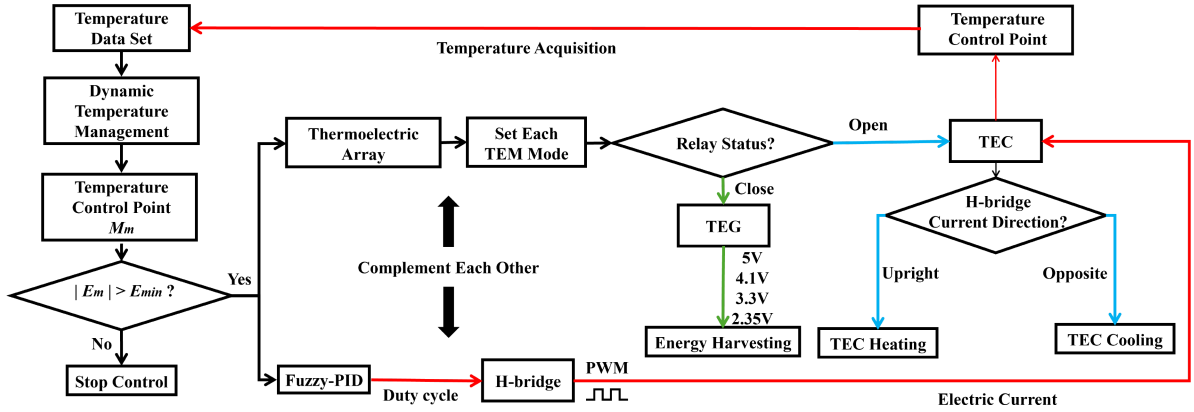


Fig. 10. Flow chart of dynamic temperature management algorithm.

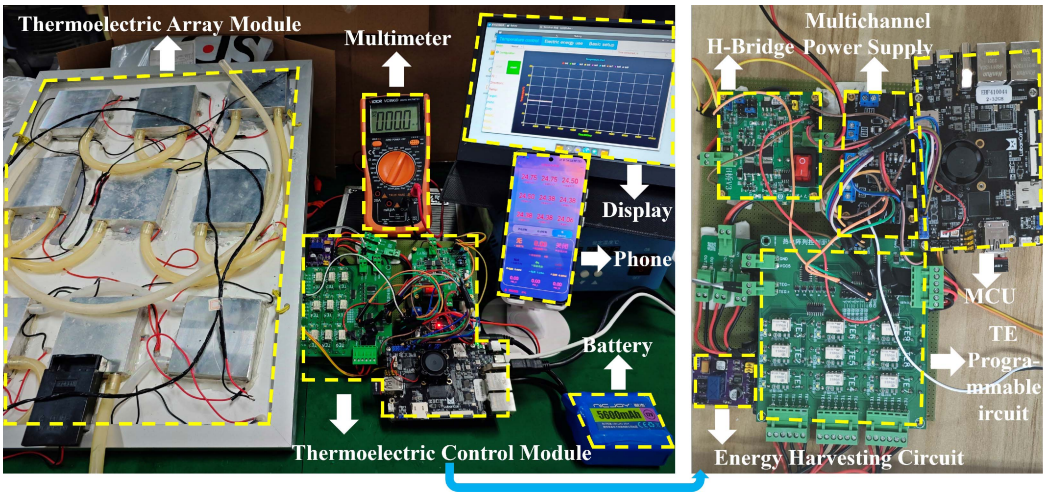


Fig. 11. Experimental setup.

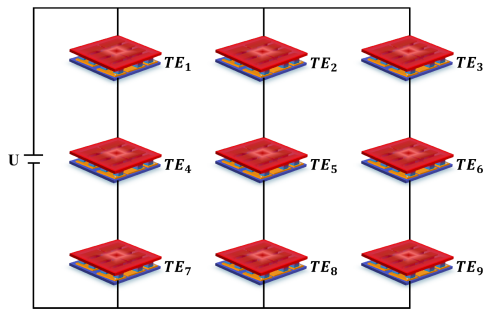


Fig. 12. Traditional connection.

causes $\xi$ to drop to a minimum of 0.1168, thereby reducing the system's effective COP. Furthermore, the total temperature error rebounds, ultimately reaching $E_{\text{total}} = 147.09$ °C [see Fig. 13(c)], with a prolonged regulation time of 511 s. These results highlight the conventional mode's inherent challenge in reconciling localized cooling with global thermal equilibrium.

In contrast, the array control mode effectively addresses the aforementioned issues through a three-stage coordinated regulation process [see Fig. 13(e)]. During the transient response phase (0–56 s), distributed cooling dominated by proportional control rapidly reduces $E_{\text{total}}$. In the transition phase (56–195 s), integral compensation is introduced to gradually converge the overall temperature. After 195 s, differential control suppresses thermal diffusion oscillations, ultimately achieving a quasi-equilibrium state with $E_{\text{total}} = 1.72$ °C in just 251 s [see Fig. 13(b)]. This approach elevates the peak $\xi$ to 383.6154, significantly enhancing system COP.

### C. Performance Comparison

As illustrated in Fig. 14(a), the array control mode employs a single TEM-TEC concentrated driving strategy ($D(k) = 1$) in the initial phase, utilizing high $I_{\text{TEC}}$ density to rapidly converge $\Delta E_m$. In contrast, the traditional mode experiences regulation lag due to uniform current distribution across the entire array. In the final phase, the array mode dynamically reallocates TEC/TEG states to achieve multiregion temperature equilibrium, reducing the adjustment time by 50.88% compared to the traditional mode. In contrast, the traditional mode, restricted by

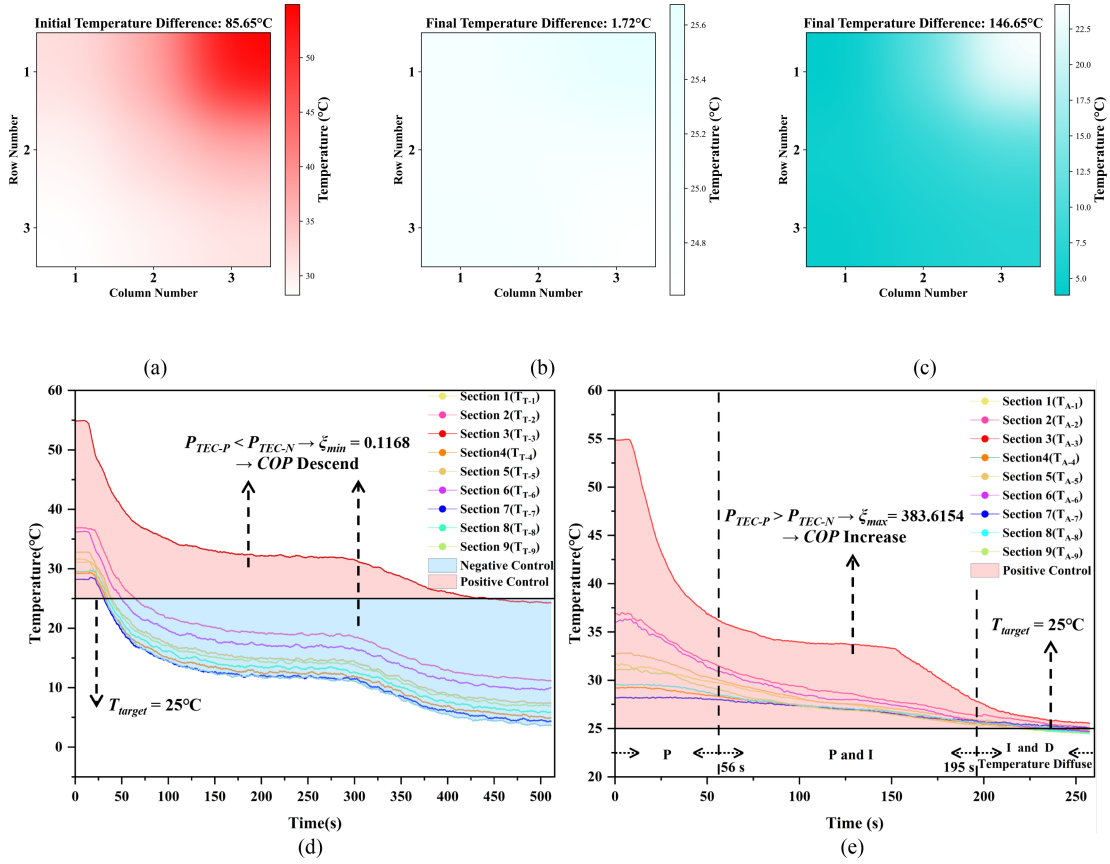


Fig. 13. Temperature variation curves and distribution. (a) Initial temperature distribution. (b) Final temperature distribution in array mode. (c) Final temperature distribution in traditional mode. (d) Traditional control mode. (e) Array control mode.

TABLE IV
PERFORMANCE COMPARISON OF TEA RELATED STUDIES

| Parameter | Buchalik et al. [17] | Kwan et al. [25] | Kim et al. [15] | **Comparative experiment** | **This work** |
|---|---|---|---|---|---|
| System Composition | TEC | TEC+TEG | TEC+TEG | **TEC** | **TEM->(TEC+TEG)** |
| TEM Connection Mode | Series or Parallel | Series-Parallel | Multistage | **Series-parallel** | **Programmable Array** |
| Temperature Control Mode | Independent Optimization Module | FLC Logic + MPPT | Energy Reuse | **Fuzzy-PID** | **Hotspot Tracking + Fuzzy-PID** |
| Temperature Range ($\Delta T$)/(°C) | 25 | 51 | 19 | **30** | **30** |
| Spend Time ($\Delta t$)/(s) | 14 400 | 4000 | 250 | **511** | **251** |
| Response Speed ($\Delta T/\Delta t$)/(°C/s) | $1.74\times10^{-3}$ | $1.275\times10^{-2}$ | $7.6\times10^{-2}$ | **$5.87\times10^{-2}$** | **$1.195\times10^{-1}$** |
| $E_{total}$ (MIN)/(°C) | / | > 5 | / | **147.09** | **1.72** |
| $P_{TEC}$ (MAX)/(W) | 100 | 500 | 55 | **36** | **36** |

its fixed TEC function, leads to localized heat accumulation, resulting in convergence only within a single region.

Analyzing $P_{\mathrm{TEC}}$ and efficiency $\eta$ [see Fig. 14(b)], the array mode exhibits a $P_{\mathrm{TEC}\text{-}P}$ ratio of 99.89% ($P_{\mathrm{TEC}\text{-}N} = 0.11\%$), with a substantial $\xi$ improvement and a maximum $\eta$ difference of 92.57%, significantly outperforming the traditional mode ($P_{\mathrm{TEC}\text{-}N} = 89.54\%$, $\xi \approx 0$). This advantage arises from the dynamic TEC/TEG switching strategy, which eliminates power backflow losses caused by global TEC operation in the traditional mode (where $P_{\mathrm{TEC}-P}$ is only 10.46%) and enhances single-TEM power optimization in near-equilibrium states, thereby maximizing $\eta$.

Table IV compares the temperature management performance of TEA systems proposed in recent years. The array mode achieves a response speed of 0.1195 °C/s, representing a 57.2% improvement over Kim et al.'s scheme (0.076 °C/s). Moreover, it completes a 30 °C temperature adjustment within 251 s using only 36 W of cooling power, improving efficiency by 104% compared to traditional series-parallel systems. Temperature control accuracy is enhanced to 1.72 °C through the

TABLE V
PERFORMANCE COMPARISON OF TEGS ARRAY RELATED STUDIES

| Parameter | Pourhoseini et al. [12] | Goswami et al. [21] | Lan et al. [13] | **This work** |
|---|---|---|---|---|
| Energy Harvesting Mode | Reconfigurable + Response Surface Methodology | Reconfigurable + Heat Recovery System | Reconfigurable + Staggered Fins Enhance Thermal Contact | **Programmable Array** |
| Coverage Area ($cm^2$) | 576 | 2500 | 480 | **128** |
| $\Delta T$ (MAX)/(°C) | 1509.85 | 46.3 | 220 | **30** |
| $P_{TEG}$(MAX)/(W) | 11.3 | 7.438 | 7 | **0. 278** |
| Power Density (MAX)/($W/cm^2K$) | $1.299\times10^{-5}$ | $6.43\times10^{-5}$ | $6.63\times10^{-5}$ | **$7.24\times10^{-5}$** |

The boldface indicates the experimental data presented in this work.

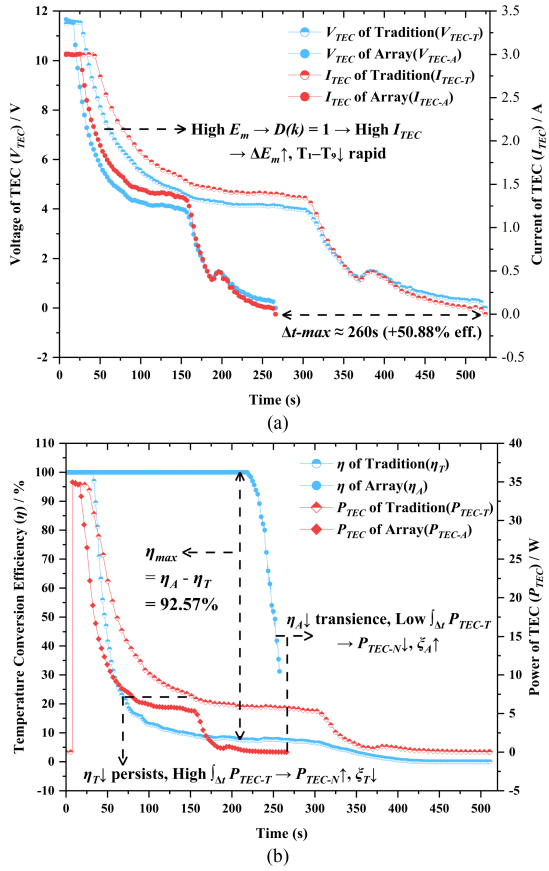


Fig. 14. (a) Comparison of I-V characteristics of TEC under different control modes. (b) Comparison of $\eta$-$P_{TEC}$ under different control modes.

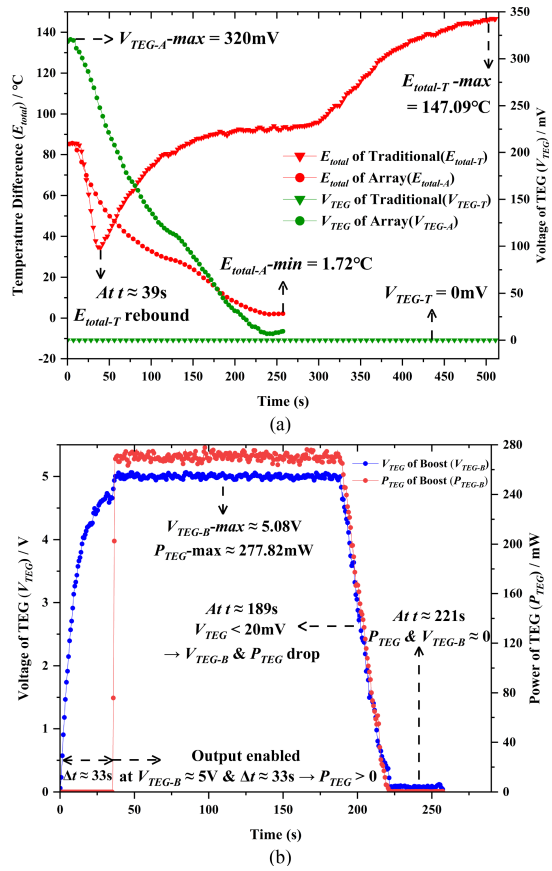


Fig. 15. (a) Comparison of $E_{\text{total}}$-$V_{\text{TEG}}$ under different control modes. (b) Comparison of V-P characteristics of TEG after boost under array mode.

implementation of dynamic topology programmable technology, and a deviation reduction of 98.8% is achieved relative to the baseline experiment (147.09 °C).

Fig. 15(a) illustrates the differences in energy recovery between the two modes. In the traditional mode, full TEC operation leads to $V_{\text{TEG}} = 0$, eliminating waste heat recovery and causing an $E_{\text{total}}$ rebound at 39 s due to temperature overshoot. In contrast, the array mode leverages a TEG series topology to achieve peak energy harvesting at $V_{\text{TEG}} = 320$ mV. As depicted in the voltage-power (V-P) characteristics of Fig. 15(b), integrating the LTC3108 ultra-low-voltage boost module (startup threshold: 20 mV) enables the system to perform constant-voltage charging at $V_{\text{TEG-}B} = 5$ V within $\Delta t = 33$ s via a 470 $\mu$F supercapacitor and charge pump (voltage ripple $< 1.6\%$). This circuit effectively mitigates voltage drops caused by pulse loads and ensures continuous power output when $V_{\text{TEG}} > 20$ mV, reaching a peak $P_{\text{TEG-}B}$ of 277.82 mW. The energy buffering mechanism guarantees stable power supply during dynamic thermal regulation, resolving the issue of unidirectional energy consumption in conventional TEA systems.

Table V compares the energy harvesting performance of recently developed TEG systems. With a constrained coverage area (128 $cm^2$) and a moderate temperature difference ($\Delta T = 30$ °C), the system achieves a power density of $7.24 \times 10^{-5}$ W/cm$^2$K, marking a 12.6% improvement over Goswami et al.'s heat recovery system ($6.43 \times 10^{-5}$ W/cm$^2$K) and exhibiting notable efficiency advantages over conventional static enhancement structures, such as Lan et al.'s staggered fin configuration. While the maximum temperature difference and

power output (0.278 W) fall short of large-scale systems (e.g., Pourhoseini's design), the energy density per unit temperature difference is enhanced by a factor of 5.6.

## V. Conclusion

This study proposes an intelligent control system based on a programmable TEM array, integrating a fuzzy-PID algorithm with a tri-state dynamic topology (cooling/heating/energy recovery). The system achieves a global temperature control accuracy of 1.72 °C in a nonuniform thermal field, representing a 98.8% improvement over conventional methods, with a 50.88% reduction in convergence time and a response rate of 0.1195 °C/s. By incorporating an LTC3108 ultra-low voltage boost circuit, the system converts waste heat voltage (peak 320 mV) into a 5-V dc output (ripple $< 1.6\%$), achieving a power density of $7.24 \times 10^{-5}$ W/cm$^2$K. The dynamic switching strategy reduces ineffective heat transport power consumption $P_{\mathrm{TEC}\text{-}N}$ to 0.11%, increases the peak energy efficiency factor $\xi$ to 383.6, and enhances temperature conversion efficiency $\eta$ by 92.57%. This approach overcomes the limitations of conventional thermoelectric systems in terms of function rigidity and energy imbalance, offering a highly efficient and energy-synergistic solution for semiconductor cooling, industrial thermal management, and other applications.

## References


[1] Y. Cao et al., "Optimal energy management for multi-microgrid under a transactive energy framework with distributionally robust optimization," *IEEE Trans. Smart Grid*, vol. 13, no. 1, pp. 599–612, Jan. 2022.

[2] N. Xu, Y. Zhu, R. Yang, X. Chen, and C.-Y. Su, "Adaptive fault-tolerant control for a 2-body point absorber wave energy converter against actuator faults: An iterative learning control approach," *IEEE Trans. Sustain. Energy*, vol. 14, no. 3, pp. 1664–1675, Jul. 2023.

[3] X. Chen et al., "Adaptive hybrid model-enabled sensing system (HMSS) for mobile fine-grained air pollution estimation," *IEEE Trans. Mobile Comput.*, vol. 21, no. 6, pp. 1927–1944, Jun. 2022.

[4] S. Zhu et al., "Estimating near-surface concentrations of major air pollutants from space: A universal estimation framework LAPSO," *IEEE Trans. Geosci. Remote Sens.*, vol. 61, 2023, Art. no. 4101011.

[5] Y. Shi, X. Cui, L. Qi, X. Zhang, X. Li, and H. Shen, "A novel energy harvesting method for online monitoring sensors in HVdc overhead line," *IEEE Trans. Ind. Electron.*, vol. 70, no. 2, pp. 2139–2143, Feb. 2023.

[6] A. M. Abomazid, N. A. El-Taweel, and H. E. Z. Farag, "Optimal energy management of Hydrogen energy facility using integrated battery energy storage and solar photovoltaic systems," *IEEE Trans. Sustain. Energy*, vol. 13, no. 3, pp. 1457–1468, Jul. 2022.

[7] X. Wu, J. Liu, Y. Men, B. Chen, and X. Lu, "Optimal energy storage system and smart switch placement in dynamic microgrids with applications to marine energy integration," *IEEE Trans. Sustain. Energy*, vol. 14, no. 2, pp. 1205–1216, Apr. 2023.

[8] N. Wang, J. Tang, H.-S. Shan, H.-Z. Jia, R.-L. Peng, and L. Zuo, "Efficient power conversion using a PV-PCM-TE system based on a long time delay phase change with concentrating heat," *IEEE Trans. Power Electron.*, vol. 38, no. 9, pp. 10729–10738, Sep. 2023.

[9] Y. Zhang, V. Cheng, D. S. Mallapragada, J. Song, and G. He, "A model-adaptive clustering-based time aggregation method for low-carbon energy system optimization," *IEEE Trans. Sustain. Energy*, vol. 14, no. 1, pp. 55–64, Jan. 2023.

[10] Y. Wang, J. Hu, and N. Liu, "Energy management in integrated energy system using energy–carbon integrated pricing method," *IEEE Trans. Sustain. Energy*, vol. 14, no. 4, pp. 1992–2005, Oct. 2023.

[11] Z. Wu et al., "Sharing economy in local energy markets," *J. Modern Power Syst. Clean Energy*, vol. 11, no. 3, pp. 714–726, 2023.

[12] S. H. Pourhoseini, M. Mohammadpoor, and M. Baghban, "RSM optimization of heat recovery from the chimneys of natural gas boilers using TEGs array: An approach for simultaneous generation of electric power and preheated water," *Energy Convers. Manage.*, vol. 331, 2025, Art. no. 119691.

[13] Y. Lan, J. Lu, and S. Wang, "An experimental study on the performance of TEGs using uniform flow distribution heat exchanger for low-grade thermal energy recovery," *Energy*, vol. 292, 2024, Art. no. 130506.

[14] Á. Valera-Albacete, F. Almonacid, P. M. Rodrigo, and E. F. Fernández, "The potential of a hybrid optical photovoltaic converter–Thermoelectric receiver to enhance conversion efficiency," *IEEE Electron Device Lett.*, vol. 44, no. 8, pp. 1360–1363, Aug. 2023.

[15] D. Kim et al., "Design and performance analyses of thermoelectric coolers and power generators for automobiles," *Sustain. Energy Technol. Assessments*, vol. 51, 2022, Art. no. 101955.

[16] S. J. Park, K. M. Bang, B. Kim, P. Ziolkowski, J.-R. Jeong, and H. Jin, "Adaptive thermoelectric cooling system for energy-efficient local and transient heat management," *Appl. Thermal Eng.*, vol. 216, 2022, Art. no. 119060.

[17] R. Buchalik, G. Nowak, and I. Nowak, "Comparative analysis and optimization of one- and two-stage cooling systems with thermoelectric cells with respect to supercooling," *Energy Convers. Manage.*, vol. 259, 2022, Art. no. 115587.

[18] X. Zhang, L. Zhan, and L. Qi, "Performance enhancement method for power electronic switch in hybrid DC circuit breaker based on partial precooling," *IEEE Trans. Power Electron.*, vol. 38, no. 1, pp. 118–122, Jan. 2023.

[19] S. Zhang, Z. Chen, Q. Bai, W. Li, and Y. Pei, "Individualization of optimal operation currents for promoting multi-stage thermoelectric cooling," *Mater. Today Phys.*, vol. 26, 2022, Art. no. 100746.

[20] Q. Wan and P. K. T. Mok, "A 14-nA, highly efficient triple-output thermoelectric energy harvesting system based on a reconfigurable TEG array," *IEEE J. Solid-State Circuits*, vol. 54, no. 6, pp. 1720–1732, Jun. 2019.

[21] R. Goswami, S. Ganguly, and R. Das, "Waste heat recovery from the biomass engine for effective power generation using a new array-based system," *Sustain. Energy Technol. Assessments*, vol. 63, 2024, Art. no. 103630.

[22] D. Yousri, A. Fathy, H. E. Z. Farag, and E. F. El-Saadany, "Optimal dynamic reconfiguration of thermoelectric generator array using RIME optimizer to maximize the generated power," *Appl. Thermal Eng.*, vol. 238, 2024, Art. no. 122174.

[23] N. Wang et al., "High efficiency thermoelectric temperature control system with improved proportional integral differential algorithm using energy feedback technique," *IEEE Trans. Ind. Electron.*, vol. 69, no. 5, pp. 5225–5234, May 2022.

[24] N. Wang, L.-L. Ni, A. Wang, H.-S. Shan, H.-Z. Jia, and L. Zuo, "High-efficiency photovoltaic-thermoelectric hybrid energy harvesting system based on functionally multiplexed intelligent thermal management," *Energy Convers. Manage.*, vol. 272, 2022, Art. no. 116377.

[25] T. H. Kwan, X. Wu, and Q. Yao, "Complete implementation of the combined TEG-TEC temperature control and energy harvesting system," *Control Eng. Pract.*, vol. 95, 2020, Art. no. 104224.

[26] A. Zhang, D. Pang, B. Wang, G. Li, and J. Lou, "Theoretical model for micro-thermoelectric coolers: Influence of coupled interfacial and thomson effects on cooling performance," *Appl. Thermal Eng.*, vol. 258, 2025, Art. no. 124750.

[27] Y. Kimura, K. Utsumi, and H. Tohmyoh, "Experimental relationship between the Seebeck and Peltier effects in thermoelectric modules based on Fe and Al metals," *Appl. Thermal Eng.*, vol. 255, 2024, Art. no. 124009.

[28] L. Ding, R. Song, S. Zhao, J. Wang, and H. A. Mantooth, "Active Peltier effect heat sink for power semiconductor device thermal stability enhancement," *IEEE Trans. Power Electron.*, vol. 38, no. 9, pp. 11507–11520, 2023.

[29] J. Xie, R. Yang, H. B. Gooi, and H. D. Nguyen, "PID-based CNN-LSTM for accuracy-boosted virtual sensor in battery thermal management system," *Appl. Energy*, vol. 331, 2023, Art. no. 120424.

[30] T. H. B. de, C. Tavares, B. P. Ferreira, and E. M. A. M. Mendes, "Fuzzy time series model based on red–black trees for stock index forecasting," *Appl. Soft Comput.*, vol. 127, 2022, Art. no. 109323.